ACS Catalysis

Letter

pubs.acs.org/acscatalysis

Promotion of Hydrogenation of Organic Molecules by Incorporating Iron into Platinum Nanoparticle Catalysts: Displacement of Inactive Reaction Intermediates

Hailiang Wang, James M. Krier, Zhongwei Zhu, Gérôme Melaet, Yihai Wang, Griffin Kennedy, Selim Alayoglu, Kwangjin An, and Gabor A. Somorjai*

Department of Chemistry, University of California, Berkeley, California 94720, United States

Materials Sciences and Chemical Sciences Divisions, Lawrence Berkeley National Laboratory, Berkeley, California 94720, United States

Supporting Information

ABSTRACT: We characterize the surface chemical states of reactants and catalysts under reaction conditions to elucidate the composition effect of platinum−iron bimetallic nanoparticles on catalytic hydrogenation of organic molecules. The catalytic hydrogenation of ethylene is drastically accelerated on the surface of 2 nm PtFe bimetallic nanoparticles as compared to pure Pt. Sum frequency generation (SFG) vibrational spectroscopy indicates that incorporation of Fe into Pt nanoparticle catalysts weakens the adsorption of ethylidyne, an inactive spectator species, on the catalyst surface. Similarly, the turnover frequency of cyclohexene hydrogenation is also significantly enhanced by incorporating Fe into Pt nanoparticle catalysts. Ambient-pressure X-ray photoelectron spectroscopy (AP-XPS) reveals the surface composition and oxidation states of the PtFe nanoparticles under reaction conditions. The oxidation state distribution of Fe responded to the gas atmosphere and the probing depth, whereas the Pt remained largely metallic in all probing conditions. This work represents a molecular level correlation between catalyst structure and catalytic performance.

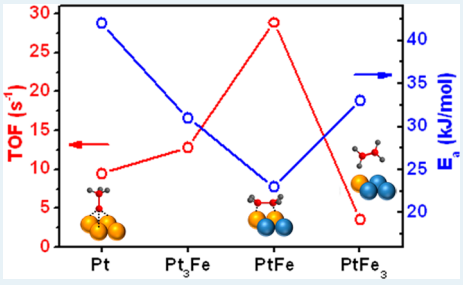

KEYWORDS: *Pt−Fe bimetallic nanoparticles, ethylene hydrogenation, cyclohexene hydrogenation, SFG, AP-XPS*

Platinum and its alloys have long been used as catalysts in the chemical industry.[1−3] Although nanosized Pt particles loaded on various types of supports have been used in heterogeneous catalysis for many decades, it was not until the synthetic capability to control size, shape, and composition of nanoparticles was developed that the correlation between structural properties and chemical properties of Pt-based nanoparticles was carefully examined.[1,4−7] Many interesting effects in chemical catalysis posed by the size, shape, and composition of Pt-based nanoparticles have been observed, which is essential toward understanding the structure−property relationship in model catalyst systems as well as advancing further optimization of catalytic activity and selectivity for challenging reactions.[8−11]

Pt−Fe bimetallic nanoparticles are promising materials for catalysis, data-storage, permanent-magnet, and biomedical applications.[12] Incorporation of Fe into the structure of Pt nanoparticles could enhance the catalytic performance for certain reactions.[13−16] For example, Pt−Fe bimetallic nanoparticles have been observed to be better catalysts than Pt nanoparticles for both the methanol oxidation reaction and the oxygen reduction reaction in direct methanol fuel cells.[13] It has also been reported that Pt−Fe bimetallic nanoparticles exhibited considerably higher activity and more desirable selectivity than Pt nanoparticles in catalysis of reactions such as selective CO oxidation in hydrogen and cinnamaldehyde hydrogenation.[14−16] Understanding of such enhancement in catalytic performance requires delicate synthesis that is able to tune the composition of the bimetallic nanoparticles while retaining their size, shape, and other important structural parameters. It is also highly desirable to characterize the chemical states on the catalyst surface under reaction conditions.

We developed a synthesis strategy that could readily produce 2 nm Pt−Fe bimetallic nanoparticles with tunable compositions by reduction of platinum(II) acetylacetonate and iron(II) acetylacetonate in ethylene glycol solution in the presence of polyvinylpyrrolidone (PVP). The obtained 2 nm Pt−Fe nanoparticles were tested for catalysis of ethylene hydrogenation reaction. It was observed that the activity was highly dependent on the composition of the nanoparticles. In particular, the PtFe nanoparticles showed ∼3 times higher activity at 25 °C and considerably lower activation energy than the Pt nanoparticles with a similar size. Sum frequency generation (SFG) vibrational spectroscopy under reaction conditions showed weaker signal of ethylidyne (a less active

Received: July 19, 2013
Revised: August 25, 2013
Published: September 18, 2013

   dx.doi.org/10.1021/cs400579j | *ACS Catal.* 2013, 3, 2371−2375

reaction intermediate compared to di-σ-ethylene) and stronger signal of di-σ-ethylene on the PtFe nanoparticle surface than on the Pt surface. Negligible ethylene intermediate adsorption on the $PtFe_3$ nanoparticle surface was observed with SFG spectroscopy, which coincides with low turnover rate. The promotion of ethylene hydrogenation on PtFe was thus believed to be due to Fe incorporation into Pt which weakened the surface adsorption of inactive intermediates. Similarly, the turnover rate of cyclohexene hydrogenation was increased on the PtFe nanoparticles compared to the Pt. Ambient-pressure X-ray photoelectron spectroscopy (AP-XPS) study of the PtFe nanoparticles revealed that while the Pt atoms remained largely metallic, the oxidation states of the Fe atoms were responsive to the gas atmosphere as well as the probing depth.

In the synthesis, we utilized ethylene glycol as the solvent and reducing agent, and PVP was used as a capping agent. When platinum(II) acetylacetonate was used as the sole precursor, Pt nanoparticles with an average size of ~6 nm were obtained (Figure 1a). Interestingly, addition of the other

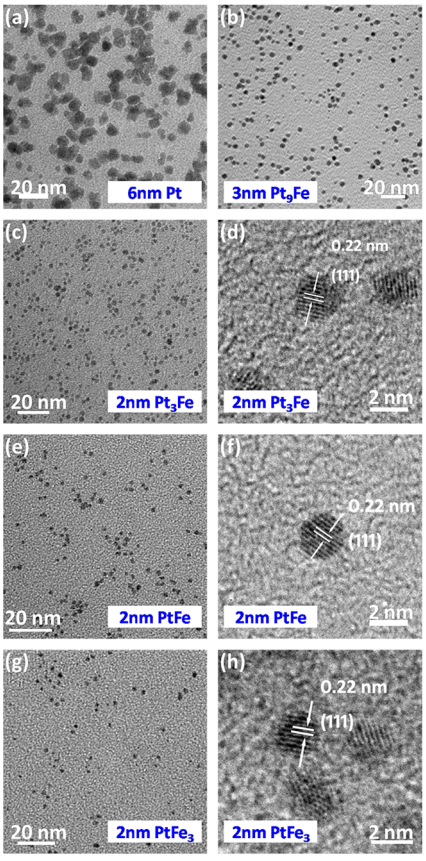

Figure 1. TEM images of Pt and Pt–Fe bimetallic nanoparticles with various compositions synthesized by changing the ratio of Pt and Fe precursors.

precursor iron(II) acetylacetonate into the system posed a size-reducing effect on the produced nanoparticles. About 3 nm size nanoparticles (Figure 1b) were produced with a precursor ratio of 9:1 (Pt/Fe). Further decreasing the Pt/Fe ratio in the precursors gave ~2 nm Pt–Fe bimetallic nanoparticles with various compositions (Figure 1c, 1e and 1g). If iron(II) acetylacetonate was used as the sole precursor, only aggregates of tiny Fe particles were obtained (Supporting Information, Figure S1). Control experiments indicated that iron(II) acetylacetonate decomposed at a lower temperature than platinum(II) acetylacetonate in ethylene glycol. It was inferred that the Fe precursor first decomposed and then the generated seeds promoted precipitation of Pt onto the Fe species, eventually leading to formation of Pt–Fe bimetallic nanoparticles with reduced size.

Our method afforded Pt–Fe nanoparticles with tunable composition and narrow size distribution. Transmission electron microscopy (TEM) images of the Pt_3Fe, PtFe, and $PtFe_3$ nanoparticles are shown in Figure 1c–h. The average sizes of the three types of Pt–Fe nanoparticles were all about 2 nm, which provided a suitable system to study the composition dependence of the Pt–Fe bimetallic nanoparticles in catalysis. High resolution TEM imaging (Figure 1d, 1f and 1h) revealed the lattice fringes of the nanoparticles, indicating the nanoparticles were in a disordered face-centered cubic structure (the Pt and Fe atoms were in random atomic arrangement). According to previous studies, high temperature annealing was needed to obtain intermetallic Pt–Fe alloy with an ordered face-centered tetragonal structure.[12,17] None of the as-prepared Pt–Fe nanoparticles were found to be ferromagnetic.

Compositions of the bimetallic nanoparticles were analyzed by energy dispersive spectroscopy (EDS) equipped on the TEM (Supporting Information, Figure S2). While the Fe atomic fractions measured by EDS came slightly lower than designed for all types of the bimetallic nanoparticles (Supporting Information, Table S1), they generally correlated well with the Pt/Fe ratios of the precursors used in the synthesis.

The 2 nm Pt–Fe bimetallic nanoparticles were compared with 2 nm Pt nanoparticles as catalysts for ethylene hydrogenation. The catalysts were prepared by depositing LB films of the nanoparticles on SiO_2 substrates.[18,19] The reactions took place in a batch reactor filled in sequence with 100 Torr of hydrogen, 10 Torr of ethylene, and 660 Torr of helium at 25 °C.[18] Turnover frequency (TOF) was calculated based on the number of total surface metal atoms derived from the size and surface density of the nanoparticles on the substrate, assuming the atomic density of the spherical nanoparticle surface was the same as that of a Pt (111) surface.[19] Activation energy was obtained by running the reactions at temperatures of 25, 40, and 55 °C.

TOF and activation energy obtained for the nanoparticles are shown in Figure 2. A TOF of ~9.5 s^{-1} was observed for the Pt nanoparticles. This was comparable to previous results of ethylene hydrogenation reactions catalyzed by Pt nanoparticles

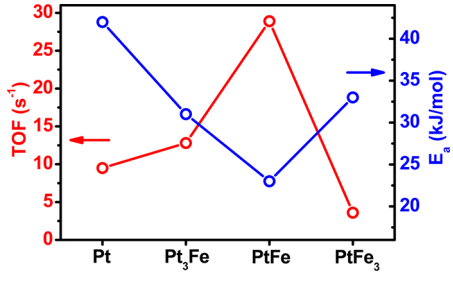

Figure 2. TOF and activation energy measured for ethylene hydrogenation reactions on 2 nm Pt and Pt–Fe nanoparticle catalysts. TOF was measured in a batch reactor with 10 Torr of C_2H_4, 100 Torr of H_2, and 660 Torr of He at 25 °C. Activation energy was calculated from reaction rates at 25, 40, and 55 °C.

dx.doi.org/10.1021/cs400579j | ACS Catal. 2013, 3, 2371–2375

under similar conditions, slightly lower compared to that for a single-crystal Pt (111) surface.[10,20,21] The difference was likely due to the assumption of a (111) surface for the nanoparticles and deactivation by PVP capping. The activation energy was calculated to be ~42 kJ/mol, which was consistent with previous studies.[10,20] The Pt_3Fe nanoparticles showed an increased TOF of ~12.8 s^{-1} and a decreased activation energy of ~31 kJ/mol compared to the Pt nanoparticles. Further increase in catalytic activity was achieved by lowering the Pt/Fe ratio in the bimetallic nanoparticles. The PtFe nanoparticles exhibited a TOF of ~28.9 s^{-1}, ~3 times higher than that of the Pt nanoparticles. The activation energy was ~23 kJ/mol, which was about 50% lower than that observed for the Pt nanoparticles. With an even lower Pt/Fe ratio, the $PtFe_3$ nanoparticles showed lower TOF (~3.6 s^{-1}) than that of the Pt nanoparticles. The activation energy was measured to be ~33 kJ/mol.

SFG vibrational spectroscopy was employed to investigate ethylene hydrogenation intermediates adsorbed on the surface of the 2 nm Pt, PtFe, and $PtFe_3$ nanoparticles, to elucidate the composition effect of the Pt−Fe bimetallic nanoparticles in ethylene hydrogenation catalysis from a molecular-level perspective. The Pt nanoparticles showed a low SFG background in H_2 atmosphere (Figure 3a black curve), owing to the disordering of PVP by H_2.[19] Under the ethylene hydrogenation reaction condition of 35 Torr of ethylene and 100 Torr of hydrogen at 20 °C, SFG vibrational peak signals at ~2875 and ~2910 cm^{-1} were detected (Figure 3a red curve), corresponding to C−H stretching modes of ethylidyne and di-σ-bonded ethylene on the catalyst surface.[22,23] The PtFe nanoparticles also showed a low background in H_2 (Figure 3b black curve). Under reaction conditions (ethylene plus hydrogen), a lower-intensity ethylidyne peak and a higher-intensity di-σ-bonded ethylene peak were observed for the PtFe nanoparticles compared to the Pt nanoparticles (Figure 3b red curve). This indicated a lower density of ethylidyne and a higher density of di-σ-bonded ethylene adsorbed on the PtFe nanoparticle surface than on the Pt surface. This could explain the higher catalytic activity of the PtFe nanoparticles compared to Pt since ethylidyne has been identified as a relatively inactive intermediate in ethylene hydrogenation (Figure 3e).[22,23] The displacement of ethylidyne by Fe incorporation into Pt could be due to a geometric effect of removing the 3-fold Pt sites where ethylidyne resides on the surface or an effect of electronic structure modification.

Unlike the Pt and PtFe nanoparticles, the $PtFe_3$ nanoparticles showed a high background in H_2, with the SFG peaks corresponding to the vibrational features of PVP (Figure 3c black curve). When the surface was rich in Fe instead of Pt, disordering of PVP by H_2 was much less effective. Switching to the ethylene hydrogenation reaction condition had no evident effect on the SFG vibrational spectrum (Figure 3c red curve), which could suggest weak interactions between ethylene species and the $PtFe_3$ nanoparticle surface. However, the large SFG background from PVP made it difficult to tell spectral changes induced by ethylene. For this reason, we treated the $PtFe_3$ nanoparticles with UV-ozone to remove PVP.[19] The SFG background signal in H_2 was significantly reduced after UV-ozone treatment (Figure 3d black curve), indicating extensive PVP removal. The cleaned nanoparticles were then probed by SFG vibrational spectroscopy under ethylene hydrogenation reaction conditions, and again, no ethylene intermediates were observed (Figure 3d red curve). It was confirmed that ethylene

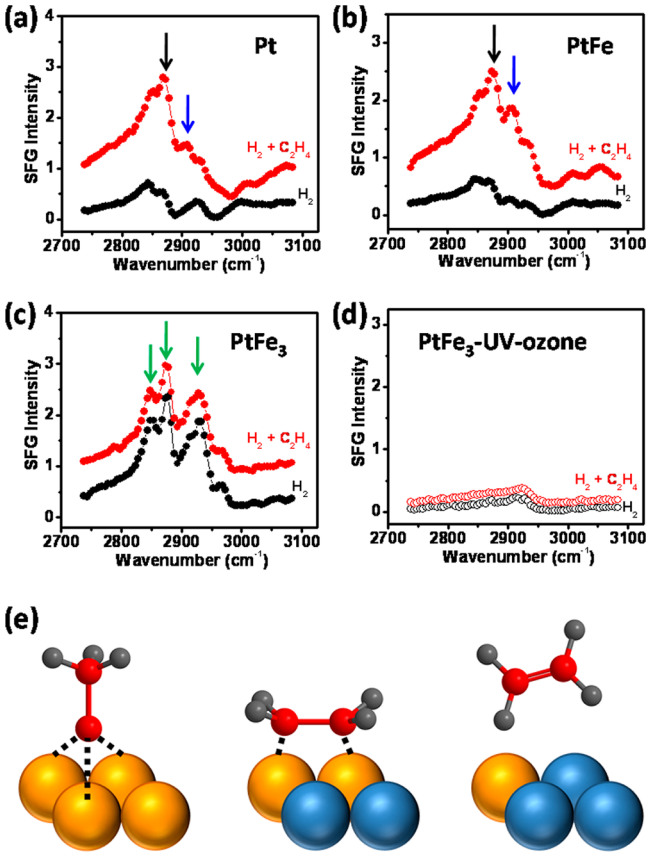

Figure 3. SFG vibrational spectroscopy study of ethylene intermediates adsorbed on the surface of Pt, PtFe, and $PtFe_3$ nanoparticles under hydrogenation reaction conditions. (a–d) SFG vibrational spectra of 2 nm (a) Pt, (b) PtFe, (c) $PtFe_3$, and (d) UV-ozone treated $PtFe_3$ nanoparticles obtained at 20 °C under hydrogen and ethylene hydrogenation conditions. The cell was first filled with 100 Torr of H_2 and 660 Torr of Ar (black curves). Then the cell was evacuated and filled with 35 Torr of C_2H_4, 100 Torr of H_2, and 625 Torr of Ar (red curves). Black and blue arrows in (a) and (b) mark the vibrational frequencies of ethylidyne (~2875 cm^{-1}) and di-σ-bonded ethylene (~2910 cm^{-1}) adsorbed on the catalyst surface, respectively. The green arrows in (c) mark the vibrational frequencies of PVP on the nanoparticle surface. (e) Schematic illustration of ethylidyne adsorbed on Pt surface (left), di-σ-ethylene adsorbed on PtFe surface (middle), and weak ethylene interaction with the $PtFe_3$ surface (right).

did not produce observable reaction intermediates on the $PtFe_3$ (Figure 3e), which was consistent with the low reaction rate.

To assess the dynamic distributions and oxidation states of the two constituent elements in the Pt−Fe bimetallic nanoparticles under reaction conditions, we performed AP-XPS measurements for the 2 nm PtFe nanoparticles in different gas atmospheres at 25 °C with various incident X-ray photon energies allowing for probing the nanoparticles at different depth levels.[24−27] Pt 4f and Fe 3p core level spectra were recorded with incident photon energy at 370, 490, and 750 eV, corresponding to photoelectron inelastic mean free path (IMFP) of 0.7, 0.9, and 1.2 nm, respectively.[28]

Deconvolution of the Pt4f and Fe 3p XPS spectra gives the oxidation state distribution of Pt and Fe.[29−33] All the fitting parameters are listed in Supporting Information, Tables S2 and S3. The Fe 3p XPS spectra were fitted by three components representing three different oxidation states without considering spin−orbit and multiplet splittings. We found the Fe atoms

dx.doi.org/10.1021/cs400579j | ACS Catal. 2013, 3, 2371−2375

on the surface were more oxidized than those in the bulk of the nanoparticles. At the IMFP of ~0.7 nm, ~38% of Fe was metallic, ~32% was Fe(II), and ~30% was Fe(III) (Figure 4a).

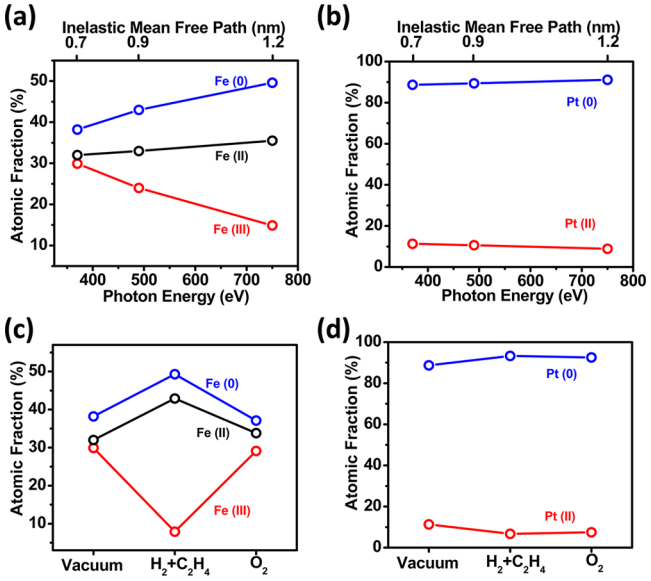

Figure 4. Probing depth and gas atmosphere dependent oxidation state distributions of Pt and Fe in 2 nm PtFe nanoparticles as probed by AP-XPS. Probing depth dependent oxidation states were probed by XPS in vacuum with incident X-ray photon energies of 370, 490, and 750 eV (corresponding to approximate IMFP of 0.7, 0.9, and 1.2 nm) at 25 °C. Gas atmosphere dependent oxidation states were probed by XPS in H_2 + C_2H_4 (100 + 10 mTorr) and O_2 (100 mTorr) environment at 25 °C with incident X-ray photon energy of 370 eV. (a) Atomic fractions of Fe species with different oxidation states in the PtFe nanoparticles vs incident X-ray photon energy and IMFP. (b) Atomic fractions of Pt species with different oxidation states in the PtFe nanoparticles vs incident X-ray photon energy and IMFP. (c) Atomic fractions of Fe species with different oxidation states at the surface of the PtFe nanoparticles under various atmospheres. (d) Atomic fractions of Pt species with different oxidation states at the surface of the PtFe nanoparticles under various atmospheres.

At larger IMFP of ~0.9 and ~1.2 nm, the percentage of Fe(0) increased to ~43% and ~50% at the expense of the decrease of Fe(III) to ~24% and ~15%, respectively (Figure 4a). The percentage of Fe(II) showed a weakly increasing trend over the increased probing depth (Figure 4a) as Fe(II) was generally considered reductive under ambient conditions. Such changes in the oxidation states of Fe were accompanied with evident changes in the shape of the Fe 3p peaks (Supporting Information, Figure S3b, d and f). In contrast, Pt remained largely metallic over the probed depth range (Figure 4b), and the shape of the Pt 4f peaks did not change with incident X-ray energy (Supporting Information, Figure S3a, c and e).

The surface chemical states of the PtFe nanoparticles were further studied in different gas environments including hydrogen-ethylene mixture and oxygen. Low incident X-ray photon energy (370 eV) allowed for probing the few layers of atoms on the nanoparticle surface. Oxidation states of the surface Fe atoms responded to the gas environments (Figure 4c), resulting in changes in the shape of the Fe 3p XPS spectra (Supporting Information, Figure S4b, d and f), whereas the Pt remained largely metallic (Figure 4d) and the shape of the Pt 4f peaks did not change with gas environment (Supporting Information, Figure S4a, c and e). In vacuum, the surface Fe atoms comprised ~38% of Fe(0), ~32% of Fe(II), and ~30% of Fe(III) (Figure 4c). Upon introduction of 100 mTorr of hydrogen and 10 mTorr of ethylene into the system, Fe(0) and Fe(II) increased to ~49% and ~43%, respectively, and Fe(III) decreased to ~8% (Figure 4c). The reduction of Fe could be due to the spillover of hydrogen atoms from the coexisting Pt atoms.[34−36] After the hydrogen and ethylene were replaced by 100 mTorr of oxygen, Fe(0) and Fe(II) were partially oxidized to Fe(III), with the oxidation state distribution of Fe recovered to that in vacuum (Figure 4c).

Despite the significant changes in Fe oxidation states, no strong dependence of Pt/Fe ratio on XPS probing depth was observed (Supporting Information, Figure S5), which was different from some other bimetallic nanoparticle systems where the elemental composition varied through the probed depth range.[24,25] Response of the surface composition to the gas environment was also weak (Supporting Information, Figure S5), because the temperature was not high enough for surface segregation to take place.[24,25]

The 2 nm Pt and Pt−Fe bimetallic nanoparticles were also tested for catalysis of cyclohexene hydrogenation reaction at 20 °C, where cyclohexane was the only product.[37] Compared to the Pt nanoparticles, the Pt−Fe nanoparticles exhibited higher activity (Figure 5). Similar to the ethylene hydrogenation case,

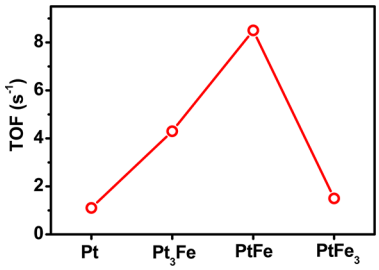

Figure 5. TOF measured for cyclohexene hydrogenation reaction over Pt and Pt−Fe nanoparticle catalysts. Reactions were carried out in a batch reactor filled with 10 Torr of cyclohexene, 200 Torr of H_2, and 560 Torr of He at 20 °C.

the PtFe nanoparticles were the most active catalyst for cyclohexene hydrogenation among all the Pt and Pt−Fe bimetallic nanoparticles. The TOF was ~8 times faster on the PtFe catalyst than on the Pt catalyst (Figure 5). The activity enhancement of Fe incorporation into Pt nanoparticle catalysts was likely realized by decreasing the surface density of reluctant intermediates such as 1,4-cyclohexadiene (requiring 4 adjacent Pt atoms) while enhancing the adsorption of more active intermediates such as di-σ-cyclohexene (requiring 2 adjacent Pt atoms) and 1,3-cyclohexadiene on the catalyst surface.[38,39]

In conclusion, we investigated the influence of composition of 2 nm Pt−Fe bimetallic nanoparticles on their catalytic performance of hydrogenation of organic molecules. The turnover rates of ethylene and cyclohexene hydrogenation were considerably increased by incorporation of Fe into Pt nanoparticle catalysts. SFG vibrational spectroscopy indicated that the activity enhancement was realized by displacing inactive reaction intermediates on the catalyst surface. AP-XPS was employed to study the dynamic composition and oxidation states of the most active 2 nm PtFe nanoparticle catalyst under reaction conditions. This work provides new insight into understanding the structure−property relationship for Pt-based bimetallic nanoparticle catalysts.

dx.doi.org/10.1021/cs400579j | ACS Catal. 2013, 3, 2371−2375

■ ASSOCIATED CONTENT

Supporting Information

Detailed experimental procedures and supplementary figures are included. This material is available free of charge via the Internet at http://pubs.acs.org.

■ AUTHOR INFORMATION

Corresponding Author

*E-mail: somorjai@berkeley.edu.

Notes

The authors declare no competing financial interest.

■ ACKNOWLEDGMENTS

This work is supported by the Director, Office of Science, Office of Basic Energy Sciences of the U.S. Department of Energy under Contract No. DE-AC02-05CH11231. H.W. acknowledges support from the Philomathia Postdoctoral Fellowship. Y.W. appreciates support from Basic Research Program of Young Scientists by National Natural Science Foundation of China and Chinese University of Hong Kong.

■ REFERENCES

(1) Somorjai, G. A.; Li, Y. *Introduction to surface chemistry and catalysis*; Wiley: Hoboken, NJ, 2010.
(2) Yu, W.; Porosoff, M. D.; Chen, J. G. *Chem. Rev.* **2012**, *112*, 5780.
(3) Greeley, J.; Stephens, I.; Bondarenko, A.; Johansson, T. P.; Hansen, H. A.; Jaramillo, T.; Rossmeisl, J.; Chorkendorff, I.; Nørskov, J. K. *Nat. Chem.* **2009**, *1*, 552.
(4) Shiju, N. R.; Guliants, V. V. *Appl. Catal., A* **2009**, *356*, 1.
(5) Li, Y. M.; Somorjai, G. A. *Nano Lett.* **2010**, *10*, 2289.
(6) Wang, D.; Li, Y. *Adv. Mater.* **2011**, *23*, 1044.
(7) Gu, J.; Zhang, Y. W.; Tao, F. *Chem. Soc. Rev.* **2012**, *41*, 8050.
(8) Alayoglu, S.; Aliaga, C.; Sprung, C.; Somorjai, G. *Catal. Lett.* **2011**, *141*, 914.
(9) Narayanan, R.; El-Sayed, M. A. *Nano Lett.* **2004**, *4*, 1343.
(10) Tsung, C.-K.; Kuhn, J. N.; Huang, W.; Aliaga, C.; Hung, L.-I.; Somorjai, G. A.; Yang, P. *J. Am. Chem. Soc.* **2009**, *131*, 5816.
(11) Xu, D.; Bliznakov, S.; Liu, Z.; Fang, J.; Dimitrov, N. *Angew. Chem.* **2010**, *122*, 1304.
(12) Sun, S. H. *Adv. Mater.* **2006**, *18*, 393.
(13) Xiang, D.; Yin, L. *J. Mater. Chem.* **2012**, *22*, 9584.
(14) Yin, J.; Wang, J. H.; Zhang, T.; Wang, X. D. *Catal. Lett.* **2008**, *125*, 76.
(15) Guo, Z.; Chen, Y. T.; Li, L. S.; Wang, X. M.; Haller, G. L.; Yang, Y. H. *J. Catal.* **2010**, *276*, 314.
(16) Liu, Z.; Tan, L. X.; Li, J.; Lv, C. *New J. Chem.* **2013**, *37*, 1350.
(17) Yu, C. H.; Caiulo, N.; Lo, C. C. H.; Tam, K.; Tsang, S. C. *Adv. Mater.* **2006**, *18*, 2312.
(18) Baker, L. R.; Kennedy, G.; Van Spronsen, M. A.; Hervier, A.; Cai, X.; Chen, S.; Wang, L.-W.; Somorjai, G. A. *J. Am. Chem. Soc.* **2012**, *134*, 14208.
(19) Krier, J. M.; Michalak, W. D.; Baker, L. R.; An, K.; Komvopoulos, K.; Somorjai, G. A. *J. Phys. Chem. C* **2012**, *116*, 17540.
(20) Rioux, R. M.; Song, H.; Hoefelmeyer, J. D.; Yang, P.; Somorjai, G. A. *J. Phys. Chem. B* **2005**, *109*, 2192.
(21) Kuhn, J. N.; Tsung, C. K.; Huang, W.; Somorjai, G. A. *J. Catal.* **2009**, *265*, 209.
(22) Cremer, P. S.; Su, X.; Shen, Y. R.; Somorjai, G. A. *J. Am. Chem. Soc.* **1996**, *118*, 2942.
(23) Kweskin, S.; Rioux, R.; Song, H.; Komvopoulos, K.; Yang, P.; Somorjai, G. *ACS Catal.* **2012**, *2*, 2377.
(24) Tao, F.; Grass, M. E.; Zhang, Y. W.; Butcher, D. R.; Aksoy, F.; Aloni, S.; Altoe, V.; Alayoglu, S.; Renzas, J. R.; Tsung, C. K.; Zhu, Z. W.; Liu, Z.; Salmeron, M.; Somorjai, G. A. *J. Am. Chem. Soc.* **2010**, *132*, 8697.
(25) Tao, F.; Grass, M. E.; Zhang, Y. W.; Butcher, D. R.; Renzas, J. R.; Liu, Z.; Chung, J. Y.; Mun, B. S.; Salmeron, M.; Somorjai, G. A. *Science* **2008**, *322*, 932.
(26) Grass, M. E.; Karlsson, P. G.; Aksoy, F.; Lundqvist, M.; Wannberg, B.; Mun, B. S.; Hussain, Z.; Liu, Z. *Rev. Sci. Instrum.* **2010**, *81*, 053106.
(27) Qadir, K.; Joo, S. H.; Mun, B. S.; Butcher, D. R.; Renzas, J. R.; Aksoy, F.; Liu, Z.; Somorjai, G. A.; Park, J. Y. *Nano Lett.* **2012**, *12*, 5761.
(28) Jablonski, A.; Powell, C. *Surf. Sci.* **2012**, *606*, 644.
(29) Sevilla, M.; Sanchís, C.; Valdés-Solís, T.; Morallón, E.; Fuertes, A. *Electrochim. Acta* **2009**, *54*, 2234.
(30) Murugesan, M.; Bea, J.; Yin, C.-K.; Nohira, H.; Ikenaga, E.; Hattori, T.; Nishijima, M.; Fukushima, T.; Tanaka, T.; Miyao, M. *J. Appl. Phys.* **2008**, *104*, 074316.
(31) Yamashita, T.; Hayes, P. *Appl. Surf. Sci.* **2008**, *254*, 2441.
(32) Wang, J.; Mao, B.; White, M.; Burda, C.; Gole, J. *RSC Adv.* **2012**, *2*, 10209.
(33) Sasaki, K.; Blowes, D. W.; Ptacek, C. J. *Geochem. J.* **2008**, *42*, 283.
(34) Dutta, G.; Waghmare, U. V.; Baidya, T.; Hegde, M. S. *Chem. Mater.* **2007**, *19*, 6430.
(35) Yu, W. Q.; Wu, B. S.; Xu, J.; Tao, Z. C.; Xiang, H. W.; Li, Y. W. *Catal. Lett.* **2008**, *125*, 116.
(36) Xu, H.; Fu, Q.; Yao, Y.; Bao, X. *Energy Environ. Sci.* **2012**, *5*, 6313.
(37) Rioux, R.; Hsu, B.; Grass, M.; Song, H.; Somorjai, G. A. *Catal. Lett.* **2008**, *126*, 10.
(38) Su, X.; Shen, Y. R.; Somorjai, G. A. *Chem. Phys. Lett.* **1997**, *280*, 302.
(39) Su, X.; Kung, K.; Lahtinen, J.; Shen, R. Y.; Somorjai, G. A. *Catal. Lett.* **1998**, *54*, 9.